Topological Fermi arcs in superfluid ^{3}He

M. A. Silaev[1] and G. E. Volovik[2,3]
[1]*Institute for Physics of Microstructures RAS, 603950 Nizhny Novgorod, Russia*
[2]*Low Temperature Laboratory, Aalto University, P.O. Box 15100, 00076 Aalto, Finland*
[3]*L. D. Landau Institute for Theoretical Physics, 117940 Moscow, Russia*
(Received 21 September 2012; revised manuscript received 2 December 2012; published 20 December 2012)

We consider fermionic states bound on domain walls in a Weyl superfluid ^{3}He-A and on interfaces between ^{3}He-A and a fully gapped topological superfluid ^{3}He-B. We demonstrate that in both cases the fermionic spectrum contains Fermi arcs that are continuous nodal lines of energy spectrum terminating at the projections of two Weyl points to the plane of surface states in momentum space. The number of Fermi arcs is determined by the index theorem that relates bulk values of the topological invariant to the number of zero-energy surface states. The index theorem is consistent with an exact spectrum of Bogolubov-de Gennes equation obtained numerically, meanwhile, the quasiclassical approximation fails to reproduce the correct number of zero modes. Thus we demonstrate that topology describes the properties of the exact spectrum beyond the quasiclassical approximation.

DOI: 10.1103/PhysRevB.86.214511 PACS number(s): 67.30.hp

I. INTRODUCTION

Chiral Weyl fermions represent the fermionic sector in the standard model of particle physics. The point nodes in the spectrum of chiral quarks and leptons are topologically protected as well as their condensed matter counterparts, which are called Dirac or Weyl points (on the topology of Weyl points in particle physics and condensed matter see, e.g., Refs. 1–5).

The nodal topological systems with Weyl fermions demonstrate different types of the bulk-surface and the bulk-vortex correspondence. Due to the bulk-vortex correspondence, the cores of some vortices in the Weyl superfluid ^{3}He-A contain a dispersionless branch of bound states with zero energy, which is a one-dimensional flat band, discussed by Kopnin and Salomaa in 1991.[6] The end points of this flat band are determined by the projections of Weyl points to the direction of vortex axis (see Refs. 7 and 8 for the topological origin of this flat band and Refs. 9–12 for discussion of the topological flat bands in general). Due to the bulk-surface correspondence, the surface of a system with Weyl points contains another exotic object—the Fermi arc—the 1D Fermi line in the 2D momentum space, which terminates on the projections of two Weyl points to the plane of the surface. The Fermi arc on the surface of ^{3}He-A shown in Fig. 2(a) has been considered in Ref. 13 and that on the surface of topological semimetals with Weyl points in Refs. 14–16. The flat band in the vortex core and the Fermi arc on the surface are momentum-space analogs of the real-space Dirac string terminating on two magnetic monopoles.[9]

Fermi arcs appear also at the interface that separates two degenerate states of ^{3}He-A with the opposite directions of the orbital anisotropy vector $\hat{\mathbf{l}}$ (in chiral superfluid ^{3}He-A vector $\hat{\mathbf{l}}$ determines the orientation of a spontaneous orbital angular momentum of this anisotropic liquid and also determines the positions $\mathbf{p} = \pm p_F \hat{\mathbf{l}}$ of two Weyl points on the Fermi surface with topological charges $N_3 = \pm 2$, if spin degeneracy is taken into account). Bound states emerging at one of the representatives of such interface—the continuous $\hat{\mathbf{l}}$-soliton—have been calculated in Ref. 17. Here, we consider bound states emerging on the singular domain wall in ^{3}He-A discussed in Refs. 18 and 19. Zero-energy edge states on such domain wall in a thin film of ^{3}He-A and the topological bulk-edge correspondence for this $2+1$ system were considered in Ref. 20. Fermi arcs emerging in the $3+1$ system form a special configuration in momentum space, see Fig. 2(b). We also consider Fermi arcs emerging at the interface between two topologically different quantum vacua: the ^{3}He-A with Weyl points and the fully gapped ^{3}He-B, which also has nontrivial topology in momentum space[12,21–23] (AB interface).

The Fermi arcs in superfluid ^{3}He solitons studied in the present paper differ qualitatively from that existing in other systems such as the surface of ^{3}He-A and Weyl semimetals. The reason is that they can be obtained ultimately beyond the quasiclassical approximation. It was found that the quasiclassical approximation yields a large number of spectrum branches which intersect the Fermi level.[17,25] The number of such branches depends on the parameters of the solition in contradiction with the topological index theorem. We show that the reason for this contradiction is that the quasiclassical Bogoluibov-de Gennes (BdG) equations inherently miss the normal reflection of quasiparticles from the spatially inhomogeneous superfluid order parameter and take into account only Andreev reflection. Thus the system of quasiclassical BdG equations is often called the system of Andreev equations. As we will discuss below, the normal reflection is crucial to describe the Fermi arcs in superfluid ^{3}He solitons. In this case, fermionic zero-energy states are realized on the quasiparticle trajectories passing at the small sliding angle to the soliton plane. For such trajectories, the normal reflection is strongly enhanced and change qualitatively the behavior of spectral branches near the zero-energy points on Fermi arcs. Here, we find numerically exact solutions of the spectral problems for BdG equations that confirm the topological index theorem predictions. Thus our results demonstrate that the topological bulk-edge correspondence describes the properties of the exact spectrum of localized boundary states, which in some cases are missed in the quasiclassical approximation.

The structure of the paper is as follows. In Sec. II, we introduce the model, which is the BdG equations and the order parameter structures of domain wall in A phase and

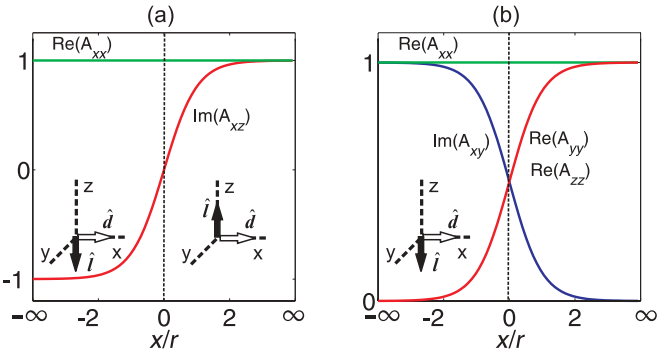

FIG. 1. (Color online) Model spatial dependencies of the order parameter components corresponding to the most symmetric and energetically preferable 1D topological defects in superfluids ^{3}He according to Refs. 18,19,31, and 32: (a) domain wall of the A phase and (b) AB interface. The order parameter is normalized to the bulk value.

AB interface. The results are presented in Sec. III where we consider at first the topological nature of Fermi arcs and then the calculations of fermionic spectrum. We discuss the failure of quasiclassical approximation to describe Fermi arcs in the fermionic spectrum of domain wall in A phase and AB interface in Sec. IV. The conclusion is given in Sec. V.

II. THE MODEL

We calculate the spectrum of eigenstates of BdG Hamiltonian describing spin-triplet p-wave superfluids/superconductors

$$\hat{H} = [\varepsilon(\hat{p}) - \mu]\hat{\tau}_3 + \hat{\tau}_1 \mathrm{Re}\hat{\Delta} - \hat{\tau}_2 \mathrm{Im}\hat{\Delta}, \tag{1}$$

where $\varepsilon(\hat{p}) = (\hat{p}_x^2 + \hat{p}_y^2 + \hat{p}_z^2)/2m$, μ is chemical potential, $\hat{p}_i = -i\nabla_i$ and $\hat{\tau}_i$ are Pauli matrices of Bogolubov-Nambu spin acting on the wave function $\psi = (u, v)^T$ with particle and hole components u and v. The gap operator is $\hat{\Delta} = A_{\alpha i}\hat{\sigma}_\alpha \hat{p}_i / p_F$, where $\hat{\sigma}_\alpha$ are Pauli matrices of spin (in ^{3}He it is nuclear spin), $p_F = \sqrt{2m\mu}$ is the Fermi momentum.

The order parameter in superfluid ^{3}He is a 3×3 matrix $A_{\alpha i}$, where the greek and latin indices correspond to the spin and orbital variables. We will consider the fermionic modes localized on different 1D order-parameter solitons, namely, the domain wall of a ^{3}He-A and the AB interface with order parameter inhomogeneity along the vector $\hat{\mathbf{n}} = \hat{\mathbf{x}}$ so that the momentum projections p_y and p_z are conserved. At first, we introduce the order-parameter structure corresponding to the discussed solitons.

A. Domain wall of A phase

We consider the configuration of one of the domain walls possible in ^{3}He-A according to the symmetry classification[19]—the one shown in Fig. 1(a). The orbital vector $\hat{\mathbf{l}}$ of the order parameter points down ($\hat{\mathbf{l}} \parallel -\hat{\mathbf{z}}$) as $x \to -\infty$ and points up ($\hat{\mathbf{l}} \parallel \hat{\mathbf{z}}$) as $x \to +\infty$. This domain wall configuration can be approximated by the following ansatz:

$$A_{\alpha i}(x) = \Delta_0 \hat{d}_\alpha [\hat{x}_i + i f(x) \hat{y}_i], \tag{2}$$

where the unit vector $\hat{\mathbf{d}}$ represents the spin part of the order parameter, which is fixed if the spin-orbit interaction is neglected, and we put $\hat{\mathbf{d}} = \hat{\mathbf{x}}$. Then the gap function is given by

$$\hat{\Delta}_{AA} = c_0 \hat{\sigma}_x [\hat{p}_x + i f(x) p_y], \tag{3}$$

where $c_0 = \Delta_0 / p_F$ is the parameter that plays the role of the longitudinal speed of light in bulk ^{3}He-A[2], $f(x)$ is an arbitrary monotonic function with asymptotic $f(\pm\infty) = \pm 1$. The topology of bound states does not depend on the details of the function $f(x)$ in Eq. (3) if it is monotonic. Note that the same model (modulo unimportant $\hat{\mathbf{d}}$ vector orientation) describes domain wall between chiral domains in $p + ip$ superconductors like Sr_2RuO_4[24] thus the fermionic spectra are identical in these cases.

B. AB interface

Let us fix the order parameter on the B phase side of the interface, i.e., at $x = +\infty$, in the following form:

$$A_{\alpha i}(x = +\infty) = \Delta_B (\hat{x}_\alpha \hat{x}_i + \hat{y}_\alpha \hat{y}_i + \hat{z}_\alpha \hat{z}_i). \tag{4}$$

The configuration of the A phase at $x \to -\infty$ can be different for different realizations of the domain wall (see, e.g., Ref. 31). They are described by the relative orientations of the vectors $\hat{\mathbf{l}}$, $\hat{\mathbf{d}}$, and $\hat{\mathbf{n}}$ (the normal to the AB interface which in our case is $\hat{\mathbf{n}} = \hat{\mathbf{x}}$). First, we shall consider the case $\hat{\mathbf{d}} = \hat{\mathbf{x}}$, $\hat{\mathbf{l}} = \hat{\mathbf{z}}$, which has the lowest energy[32]

$$A_{\alpha j}(x = -\infty) = \Delta_A \hat{x}_\alpha (\hat{x}_j - i \hat{y}_j). \tag{5}$$

We model the domain wall at the AB interface with $\Delta_A = \Delta_B = \Delta_0$ and the switching between bulk phases (4) and (5) as follows:

$$A_{xx} = \Delta_0 = \mathrm{const}, \tag{6}$$

$$A_{yy} = A_{zz} = \Delta_0 f_1(x), \tag{7}$$

$$A_{xy} = -i \Delta_0 f_2(x), \tag{8}$$

where $f_{1,2}(x)$ are arbitrary monotonic functions with asymptotics $f_1(-\infty) = 0$, $f_1(+\infty) = 1$ and $f_2(-\infty) = 1$, $f_2(+\infty) = 0$. The order parameter components (6) are shown in Fig. 1(b). Then the gap operator is given by

$$\hat{\Delta}_{AB} = c_0 \hat{\sigma}_x [\hat{p}_x - i f_2(x) p_y] + c_0 f_1(x) [\hat{\sigma}_y p_y + \hat{\sigma}_z p_z]. \tag{9}$$

III. RESULTS

A. Topology of Fermi arcs in superfluid ^{3}He

As we have mentioned in Introduction the spectrum of fermions bound to the surface of superfluid ^{3}He A is known to contain the Fermi arc.[13] Let us now compare the Fermi arcs on a domain wall in ^{3}He-A with the Fermi arc on a surface of ^{3}He-A shown in Figs. 2(a) and 2(b), correspondingly. In both cases, Fermi arcs originate from the Weyl points in the bulk spectrum. But in case of the domain wall the Weyl points exist in the bulk liquids on both sides of the wall, as a result there are two Fermi arcs in Fig. 2(b) instead of a single Fermi arc in Fig. 2(a). Topological origin of two Fermi arcs on the domain wall is demonstrated in Fig. 3. The Weyl points on two sides of the interface have the same positions in momentum space, but opposite values of topological invariant N_3.

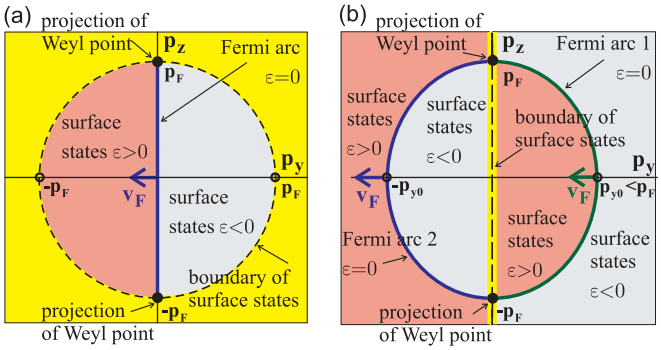

FIG. 2. (Color online) The manifold of zero energy states in p_y, p_z plane in the spectrum of bound fermions $\varepsilon(p_y, p_z) = 0$ forms (a) the Fermi arc (solid blue line) on the boundary of ^{3}He-A according to Ref. 13; (b) two Fermi arcs on the domain wall in Eq. (2). Only single spin projection is considered. Thick arrows show directions of Fermi velocity at the Fermi arcs. In (a), the Fermi arc has topological charge $N = +1$, which satisfies the index theorem following from the bulk-surface correspondence and the momentum space topology of Weyl points in bulk ^{3}He-A. Fermi arc terminates on the projections of Weyl points to the surface of ^{3}He-A. The spectrum of bound states terminates at the dashed line where the spectrum merges with the bulk spectrum. The region of continuous spectrum is shown by yellow shading. In (b), at $p_z = 0$, the Fermi velocity at the Fermi arcs is in the same direction, $\mathbf{v_F} = -v_F\mathbf{y}$, which demonstrates that both Fermi arcs have the same topological charge $N = +1$, which together satisfy the index theorem $\tilde{N}_3(\text{left}) - \tilde{N}_3(\text{right}) = +2$, in agreement with momentum space topology of Weyl points in bulk ^{3}He-A on two sides of the domain wall in Fig. 3. Fermi arcs terminate on the projections of Weyl points to the interface. The spectrum of bound states has discontinuity at $p_y = 0$ where the spectrum merges with the bulk spectrum (the edge of continuum is shown by dashed line).

The bulk spectrum in the plane with fixed p_z in momentum space has no nodes if $|p_z| \neq p_F$ and thus corresponds to the spectrum of 2D insulator. This insulator is topological for $|p_z| < p_F$, since it is described by nonzero topological invariant introduced in Refs. 27–30 for $2+1$ systems:

$$\tilde{N}_3(p_z) = \frac{1}{4\pi^2}\mathrm{tr}\left[\int dp_x dp_y d\omega G\partial_{p_x}G^{-1}G\partial_{p_y}G^{-1}G\partial_{\omega}G^{-1}\right]. \tag{10}$$

Here, G is the Green's function matrix, which in our noninteracting models is $G = (i\omega - \hat{H})^{-1}$. One has $\tilde{N}_3(|p_z| < p_F) = +1$ on one side of the wall and $\tilde{N}_3(|p_z| < p_F) = -1$ on the other side. According to the index theorem,[2,20] the difference between these two values determines the number of the zero modes at the interface between the $2+1$ topological insulators for each $|p_z| < p_F$. As a result, one has two Fermi arcs at the soliton wall.

B. Calculation of the spectrum

At first, we note that the spectral problem for the domain wall can be significantly simplified since the BdG Hamiltonian (1) with the gap operator given by Eq. (3) is proportional to the fermionic spin $\hat{\sigma}_x$. Thus we transform the quasiparticle wave function $\psi = (u, v)^T$ to remove the spin dependence of the order parameter $\tilde{u} = \hat{\sigma}_x u$, $\tilde{v} = v$, which yields the gap operator in the form

$$\hat{\Delta} = c_0[\hat{p}_x + if(x)p_y]. \tag{11}$$

Furthermore, the spectral problem for the AB interface with the gap operator given by Eq. (9) can be mapped on the case of a domain wall of the A phase. Let us transform the quasiparticle wave function components as follows: $\tilde{u} = \hat{\sigma}_x u$, $\tilde{v} = v$. We choose the spin basis $\chi_\sigma = (ip_z, \sigma_\perp p_\perp - p_y)$ of the eigenstates of the operator $\hat{\sigma}_\perp = \hat{\sigma}_z p_y - \hat{\sigma}_y p_z$ corresponding to the eigenvalues $\sigma_\perp = \pm 1$, where $p_\perp = \sqrt{p_y^2 + p_z^2}$. Then the order parameter is diagonal in spin space and has the form of

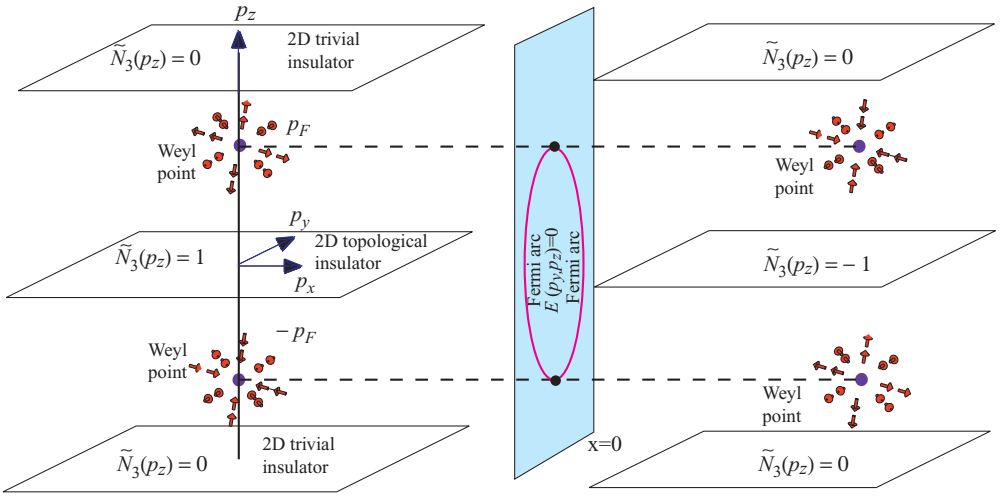

FIG. 3. (Color online) Topology of the fermionic bound states on the domain wall in ^{3}He-A. Momentum space topology of Weyl points in bulk ^{3}He-A on two sides of the wall prescribes existence of the Fermi arcs in the spectrum of the fermionic states in the soliton or at the interface between the bulk states with different positions of Weyl points. In the considered case of the domain wall, the Weyl points on two sides of the interface have the same positions in momentum space, but opposite topological invariants N_3. This leads to two Fermi arcs terminating on the projections of the Weyl points to the plane of domain wall [see Fig. 2(b)] according to the index theorem $\tilde{N}_3(\text{left}) - \tilde{N}_3(\text{right}) = 2$. This is distinct from the single Fermi arc on the surface of the ^{3}He-A in Fig. 2(a).

Eq. (11), where

$$f(x) = \sigma_\perp p_\perp f_1(x) - p_y f_2(x). \tag{12}$$

In order to obtain the bound states, the function (12) has to satisfy the condition $f(+\infty)f(-\infty) < 0$, which yields $\sigma_\perp p_y > 0$. Thus in contrast to the case of the domain wall considered above the spin degeneracy is removed since the proper spin state is determined by the condition of bound state existence.

The continuous part of the spectrum $\varepsilon_c(\mathbf{p})$ of fermionic excitations is determined by the eigenstates of Hamiltonian (1) at the bulk regions $|x| \gg r$:

$$\varepsilon_c(\mathbf{p}) = \pm\sqrt{[\varepsilon(p) - \mu]^2 + c_0^2\left(p_x^2 + p_y^2\right)}. \tag{13}$$

The states localized at the domain wall are characterized by a single discrete quantum number which enumerates the energy branches and by the two continuous quantum numbers which are the projections of the quasiparticle momentum $p_{y,z}$ onto the domain wall plane. The energy of localized states is confined within the region $|\varepsilon| < \min_{p_x} \varepsilon_c(\mathbf{p})$.

In general, the eigenvalue problem of BdG Hamiltonian (1) yields a system of differential equations which can not be solved analytically. However, there are approximate methods that can help to study qualitative features of the spectrum. First of all, we will employ the semiclassical approach[26] when the momentum operator is approximated by a number $\hat{p}_x = p_x(x)$ thus turning the differential BdG equations into the algebraic ones. In this case, the spectrum of bound states is determined by Bohr-Sommerfeld quantization of classical periodic motion between reflection points discussed in the Sec. III B1. The semiclassical approximation fails when the distance between reflection points is too small. Particularly important is the case when two Andreev reflection points come close together forming the bound state that correspond to the so called "zeroth branch" of the energy spectrum.[17,25] This case can be treated with the help of another approach—the quasiclassical approximation when one can use reduced order Andreev equations for the envelope wave functions discussed in Sec. III B2. The quasiclassical approximation in BdG equations is applicable as long as the normal reflection can be neglected. For the structures considered in the present paper, the normal reflection is crucial to describe properly the zero modes of the fermionic spectrum. This can be done only with the help of numerical solution of the exact BdG system of equations discussed in Sec. III B3.

Hereafter, we will choose the model form of Eq. (11) with $f(x) = \tanh(x/r)$ where $r \sim \xi$ is width of the domain wall and $\xi = \hbar v_F/\Delta_0$ is the coherence length where $v_F = p_F/m$ is the Fermi velocity. The fermionic spectrum in this configuration was considered in Ref. 25 in quasiclassical approximation. Here in Sec. III B3, we will implement an analysis of the fermionic spectrum beyond the quasiclassics in order to study the Fermi arcs supporting Majorana states.

1. *Semiclassical spectrum*

We begin the analysis of the spectrum of localized states from the semiclassical approximation. Provided the condition $|p_x|\xi \gg 1$ is valid we use the expression for the energy (13) substituting the local value of the order parameter. In this case, we obtain

$$\varepsilon = \pm\sqrt{\left[p_x^2/2m - \mu_x\right]^2 + c_0^2\left[p_x^2 + f^2(x)p_y^2\right]}, \tag{14}$$

where $\mu_x = \mu - (p_y^2 + p_z^2)/2m$. From Eq. (14), the function $p_x = p_x(x)$ can be found that describes semiclassical orbits in (p_x,x) phase space. In general, the orbits can have two types of stationary points determined by the nature of quasiparticle reflection.

The normal reflection occurs at the points $x = x_{1,2}^n$ defined by $p_x(x_{1,2}^n) = 0$ or, equivalently,

$$c_0 p_y f\left(x_{1,2}^n\right) = \pm\sqrt{\varepsilon^2 - \varepsilon_{n2}^2} \tag{15}$$

and exists at the energy interval $\varepsilon_{n1} > |\varepsilon| > \varepsilon_{n2}$, where $\varepsilon_{n1} = \sqrt{(c_0 p_y)^2 + \mu_x^2}$ and $\varepsilon_{n2} = |\mu_x|$. The Andreev reflection occurs at $x = x_{1,2}^a$ where $\mathrm{Im}(p_x)$ becomes nonzero:

$$c_0 p_y f\left(x_{1,2}^a\right) = \pm\sqrt{\varepsilon^2 - \varepsilon_{a2}^2}, \tag{16}$$

and exists if $\varepsilon_{a1} > |\varepsilon| > \varepsilon_{a2}$, where $\varepsilon_{a1} = c_0\sqrt{p_y^2 + 2m\mu_x - (mc_0)^2}$ and $\varepsilon_{a2} = c_0\sqrt{2m\mu_x - (mc_0)^2}$.

One can see that $\varepsilon_{n1} > \varepsilon_{a1}$ and $\varepsilon_{n2} > \varepsilon_{a2}$, therefore Eq. (14) determines two qualitatively different types of the enclosed classical orbits in (p_x,x) space. That is, for the energies (i) $\varepsilon_{n1} > |\varepsilon| > \varepsilon_{a1}$, the orbits have only normal reflection points and for (ii) $\varepsilon_{n2} > |\varepsilon| > \varepsilon_{a2}$, only Andreev reflection points. The orbits of type (i) and (ii) are shown in the Fig. 4(a) by red dashed and green solid lines correspondingly. Provided (iii) $\varepsilon_{a1} > \varepsilon_{n2}$, there is also the third regime when the orbit has both normal and Andreev reflection points, which is shown by the blue dash-dotted line in the Fig. 4. The energy spectrum is determined by the Bohr-Sommerfeld quantization

$$\oint p_x dx = 2\pi(n_s + \gamma), \tag{17}$$

where n_s is integer, $\gamma = 1/2$ for the orbits with two normal reflection points and $\gamma = 0$ for the orbits without normal reflection points.[26] Semiclassical spectral branches for $n_s = 1,2$ are shown in Fig. 4(b) by solid lines. The number of branches is doubled when the classical orbits with only Andreev reflection points merge into the single one with both normal and Andeev reflection points. The discontinuity of semiclassical branches in Fig. 4(b) is caused by the emergence of two normal reflection points on the classical orbits which change abruptly the factor γ in Bohr-Sommerfeld quantization rule (17).

From the above semiclassical consideration, we obtain that the energy of localized states is not bounded as a function of p_y and p_z. Indeed, let us consider the case (i) and assume $\sqrt{\varepsilon^2 - \mu_x^2} \ll c_0|p_y| \ll |\varepsilon|$. In this case, we can put $f(x) = x/r$ in the Eq. (14), which yields then the harmonic oscillator spectrum

$$\varepsilon_{ns}(p_y, p_z) = |\mu_x| + \omega(n_s + 1/2), \tag{18}$$

where $\omega = c_0(|p_y|/p_F r)\sqrt{2\mu/|\mu_x|}$. One can see that the Eq. (18) yields $\varepsilon > |\mu_x|$. Hence the energy branches at $\mu_x < 0$ can have arbitrary high energy when $\mu_x \to -\infty$. This tendency can be seen in the Fig. 4(b).

Besides the energy branches determined by Bohr-Sommerfeld quantization with $n_s \geqslant 1$, there exists a so-called

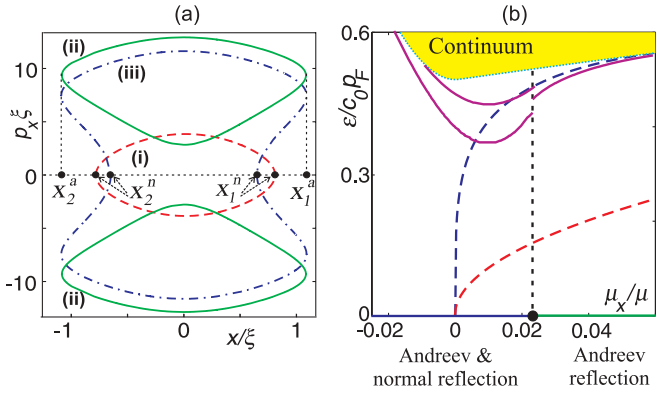

FIG. 4. (Color online) (a) Closed orbits $p_x = p_x(x)$ determined by the semiclassical Eq. (14) at the domain wall for $p_z = 0$, $p_y = 0.5p_F$, and $c_0/v_F = 2.5\ 10^{-3}$. Shown by red dashed, green solid, and blue dash-dotted curves are the regimes (i)–(iii) discussed in the text. The positions of Andreev $x_{a1,2}$ and normal $x_{n1,2}$ reflection points on the semiclassical orbits are indicated. (b) Comparison of energy spectrum given by quasiclassical and semiclassical approximations. The quasiclassical spectrum given by Eq. (24) is shown for $n_q = 0,1$ by dashed red and blue lines. The quasiclassical approximation takes into account only Andreev reflection hence the spectrum is doubly degenerate by sign(p_x). The semiclassical approach describes both Andreev and normal reflection hence the degeneracy by sign(p_x) is removed. The branches given by Bohr-Sommerfeld quantization (17) of semiclassical orbits with $n_s = 1,2$ are shown by solid magenta lines. The number of semiclassical branches is doubled due to the normal reflection when the Andreev orbits shown in (a) by green solid lines merge into the single one shown by blue dash-dotted line with both normal and Andreev reflection points.

"zeroth branch" of the spectrum that contains the zero-energy modes $\varepsilon = 0$. This branch can not be obtained from the semiclassical approach therefore a different treatment is needed.[17]

2. *Quasiclassical approximation*

To find the zeroth branch analytically, we assume the restriction $(p_x/p_F)p_x\xi \gg 1$, where $p_x = \sqrt{2m\mu_x}$ is a constant number. Qualitatively, this restriction corresponds to the regime (iii) in Fig. 4 when the deviation $\tilde{p}_x(x)$ of momentum $p_x(x) = \sqrt{2m\mu_x} + \tilde{p}_x(x)$ along the orbit is much smaller than its average value $|\tilde{p}_x| \ll \sqrt{2m\mu_x}$. In this case, we can neglect the second-order terms in $\tilde{p}_x$ still treating it as an operator so that $[\varepsilon(\hat{p}) - \mu] \approx -iv_x\partial_x$, where the projection of the Fermi velocity on the x axis is $v_x = p_x/m = \pm\sqrt{p_F^2 - p_z^2 - p_y^2}/m$. This allows to consider the regimes when the closed orbits become so small that semiclassical approximation does not apply. In particular, it allows to calculate the zeroth branch that appears when the distance between Andreev reflection points is much smaller than the coherence length ξ. In this way, one obtains a system of abridged equations for the wave function envelopes, which is called the system of quasiclassical Andreev equations. The quasicalssical approximation inherently misses the normal reflection of particles from the order parameter inhomogeneities. As we will see below, the normal reflection is crucial to describe the Fermi arcs and Majorana states at the domain wall considered. However, away from the Fermi arcs, the quasicalssical approximation matches the exact spectrum obtained numerically.

To obtain analytical solutions of Andreev equations, first, let us introduce the transformation of the quasiparticle wave function $\psi = (u,v)^T$:

$$g_+ = v + u, \tag{19}$$

$$g_- = v - u, \tag{20}$$

so that the system of Andreev equations acquires the form

$$\begin{pmatrix} h_+ & \varepsilon + c_0 p_x \\ \varepsilon - c_0 p_x & h_- \end{pmatrix} \begin{pmatrix} g_+ \\ g_- \end{pmatrix} = 0, \tag{21}$$

where $h_\pm = -iv_x\partial_x \pm ic_0 f(x)p_y$.

The system (21) can be transformed to the decoupled second-order equations

$$\left[\partial_x^2 + U_{0+}\cosh^{-2}x\right]g_+ = Eg_+, \tag{22}$$

$$\left[\partial_x^2 + U_{0-}\cosh^{-2}x\right]g_- = Eg_-, \tag{23}$$

where $E = (r/\xi)^2 + \alpha^2 - (p_F\varepsilon/p_x\Delta_0)^2$, $U_{0+} = \alpha + \alpha^2$, $\alpha = rc_0p_y/v_x$, and $U_{0-}(p_y) = U_{0+}(-p_y)$. Equation (22) has eigenvalues

$$E_{\rm nq} = (1 + 2n_q - \sqrt{1 + 4U_{0+}})^2/4 = (n_q - \alpha)^2,$$

where $n_q \geqslant 0$ is integer, which results in the quasiclassical spectral branches[17,25]

$$\varepsilon_{\rm nq} = \pm\Delta_0\frac{|p_x|}{p_F}\sqrt{2\alpha n_q - n_q^2 + (r/\xi)^2}. \tag{24}$$

Note that the energy branches (24) are twofold degenerate with respect to the sign change of p_x projection.

The zeroth spectral branch is given by the Eq. (24) with $n_q = 0$:

$$\varepsilon_0(p_y,p_z) = c_0{\rm sign}(p_y)|p_x|. \tag{25}$$

The dependencies of zeroth branch (25) $\varepsilon_0 = \varepsilon_0(\mu_x)$ at fixed p_y and $\varepsilon_0 = \varepsilon_0(p_y)$ at fixed p_z are shown in Fig. 5 by red dashed lines and in Fig. 6 by blue dashed lines correspondingly. At $p_y = 0$, this spectral branch is discontinuous and merges the edge of continuum $\varepsilon_c = \pm c_0\sqrt{p_F^2 - p_z^2}$ at $p_y = \pm 0$.

Substituting the energy of zeroth branch into Eq. (16) for the coordinates of Andreev reflection points, we obtain $|x_{a1,2}| = p_F^{-1}(r/\xi)(p_F/|p_y|) \sim p_F^{-1}$ provided $|p_y|$ is not too small. For such a small distance between reflection points, the semiclassical approximation is not valid and therefore it can not describe the zeroth branch.

The spectral branches with $n_q > 0$ given by Eq. (24) exist only in the limited range of parameters $\sqrt{p_F/\xi} \ll |p_x| < p_x^*$, where $p_x^* = |p_y|n_q/[n_q^2 - (r/\xi)^2]$ provided that $n_q > r/\xi$. At $p_x = p_x^*$, the branch merges the continuum. This behavior is demonstrated in Fig. 4(b) where the energy branches (24) with $n_q = 0,1$ are shown by dashed red and blue lines as a function of $\mu_x = \mu - (p_y^2 + p_z^2)/2m$ for the parameters $r = \xi/2$ (width of the domain wall), $c_0/v_F = 2.5 \times 10^{-2}$ and $p_y = 0.5p_F$. The zeroth branch merges the continuum at $p_y = \pm 0$ where the spectrum Eq. (25) is discontinuous. This behavior is shown by dashed blue lines in Fig. 6.

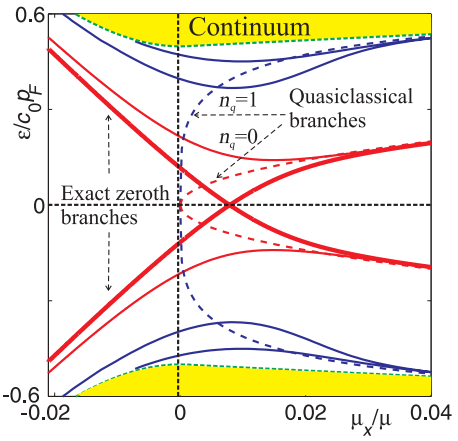

FIG. 5. (Color online) The spectrum of surface states at the A phase domain wall and the AB interface $\varepsilon = \varepsilon(\mu_x)$, where $\mu_x = \mu - (p_y^2 + p_z^2)/2m$. The parameters are $r = \xi/2$ (width of the domain wall) and $c_0/v_F = 2.5\ 10^{-2}$, $|p_y| = 0.5p_F$. Shown by solid red and blue lines are the spectral branches determined by the exact solution of BdG Eq. (1). Thick red solid lines show the zeroth branches at $p_y = \pm 0.5p_F$. Dashed lines represent quasiclassical energy branches (24) for $n_q = 0$ (red line) and $n_q = 1$ (blue line) degenerate by sign(p_x). The degeneracy by sign(p_x) is removed at the region $|\mu_x| \ll \mu$ and $\mu_x < 0$ where each quasiclassical branch splits by two modes. In accordance with general topological argument, the only one zeroth branch remains at fixed value of p_y (and spin projection σ_x for the domain wall of the A phase) shown by the red solid line. The spectrum of delocalized states is shown by yellow shading and the edge of continuum by thin dotted line.

3. *Exact spectrum near the Fermi arcs*

As pointed out by Nakahara[25] all quasiclassical branches (25) formally contain zero energy states at $p_x = 0$ but Eq. (25) is applicable if $(p_x/p_F)p_x\xi \gg 1$. In the limit $p_x \to 0$, and arbitrary values of p_y and p_z, the spectrum can be found numerically by solving the eigenvalue problem for the Eq. (21). The resulting several lowest energy spectrum branches $\varepsilon = \varepsilon(\mu_x)$ are shown in the Fig. 5 by solid red and blue lines as a function of $\mu_x = \mu - (p_y^2 + p_z^2)/2m$. Remarkably, the twofold degeneracy $p_x \to -p_x$ of the quasiclassical spectrum is broken at $0 < \mu_x \ll \mu$ and at $\mu_x < 0$. Therefore each of the quasiclassical energy branches (25) found by Nakahara splits by two modes as $\mu_x \to +0$ (and $p_x = \sqrt{2m\mu_x} \to 0$). The splitting is caused by normal reflection of quasiparticles from the order parameter spatial inhomogeneity. The normal reflection is particularly important for the quasiparticle trajectories passing almost parallel to the domain wall plane when $p_x \to 0$. In this case, the normal reflection leads to the drastic change in the spectral branches behavior near the zero-energy point shown in Fig. 5 (compare the dashed and solid lines). The influence of normal reflection on the spectrum of bond fermions was analyzed above in the framework of semiclassical approach in Sec. III B 1. Comparing the Figs. 4(b) and 5, one can see that the semiclassical approach qualitatively describes the doubling of spectral branches due to the normal reflection but gives rather large quantitative discrepancy with the exact spectrum.

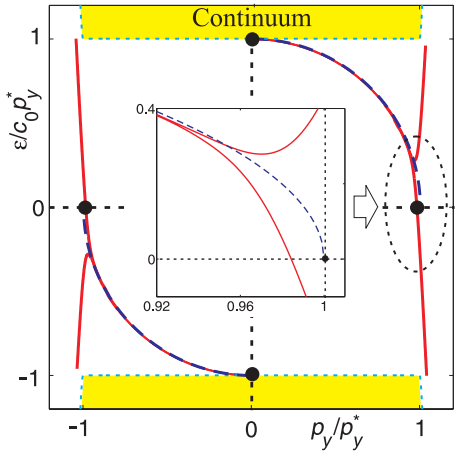

FIG. 6. (Color online) The lowest-energy spectral branches of the surface states at the domain wall of the A phase and at the AB interface as functions of p_y at fixed p_z. Shown by blue dashed line is the quasiclassical zeroth branch (25), which ends at $p_y = \pm p_y^*$, where $p_y^* = \sqrt{p_F^2 - p_z^2}$. Exact branches shown by solid red lines continue at $|p_y| > p_y^*$. At $p_y = \pm 0$, the discrete spectrum merges with continuum shown by the yellow shading. (Inset) Zoomed area demonstrating in detail the splitting of quasiclassical zeroth branch and the behavior of exact branches near the end point of quasiclassical one.

In accordance with general topological argument in Sec. III A, the only one zeroth branch remains at each fixed value of momentum projection p_y (and spin projection σ_x for the domain wall of the A phase). Exact zeroth branches for $p_y = \pm 0.5p_F$ are shown in the Fig. 5 by thick red solid lines. The spectrum in Fig. 5 is invariant with respect to the transformation $\varepsilon(p_y,\sigma) = -\varepsilon(-p_y, -\sigma)$, where $\sigma = \sigma_x$ for the case of domain wall and $\sigma = \sigma_\perp$ for that of the AB interface. Note that in contrast to the quasiclassical zeroth branch shown by red dashed line the exact zeroth branch intersects the Fermi level at finite value of $\mu_x = \mu_{x0} > 0$. This crossing point determines the positions of Fermi arcs shown in the Fig. 2(b) by blue and green solid lines. For example, the Fermi arcs cross the line $p_z = 0$ at $p_y = \pm p_{y0}$, where $p_{y0} = \sqrt{2m(\mu - \mu_{x0})} < p_F$.

Near the projection of Weyl point on $p_y p_z$ plane in the limit $p_y \to 0$ and $|p_z| \to p_F$ the behavior of zeroth branch can be found analytically using the approach of Ref. 20. We will treat the first term in the Hamiltonian (1) as perturbation. The rest of the terms form the zero-order Hamiltonian

$$\hat{H}_0 = \hat{\tau}_1 \hat{p}_x - \hat{\tau}_2 p_y f(x), \tag{26}$$

where $\hat{p}_x = -i\partial_x$. We assume the model form of the domain wall $f(x) = \tanh(x/r)$. The Hamiltonian (26) has zero-energy eigenstate with the wave function components $\psi_0 = (u_0, v_0)$,

$$u_0 = 0, \tag{27}$$

$$v_0 = N^{-1/2} \cosh^{-\alpha}(x/r), \tag{28}$$

where $\alpha = rp_y$ and $N = \int_{-\infty}^{\infty} \cosh^{-2\alpha}(x/r)dx$. The perturbation of the zero-energy level is given by

$$\varepsilon_0(p_x, p_y) = \frac{\bar{p}_x^2}{2m} - \mu_x, \tag{29}$$

where $\bar{p}_x^2 = \langle\psi_0|\hat{p}_x^2|\psi_0\rangle$. The Fermi arc is then given by

$$p_z^2 = p_F^2 - \bar{p}_x^2 - p_y^2. \tag{30}$$

In the limit $p_y \to 0$, we obtain $\bar{p}_x^2 = p_y^2$ so that the Fermi arc is given by $p_z^2 = p_F^2 - 2p_y^2$ and ends at $p_z = \pm p_F$ in accordance with general topological arguments. Equation (29) describes analytically the zeroth branch of the spectrum shown by thick red lines in Fig. 5 near the projections of Weyl points on $p_y p_z$ plane.

The splitting of quasiclassical zeroth branches $\varepsilon = \varepsilon_0(p_y)$ at fixed value of $p_z = 0$ is shown in Fig. 6. Red solid lines is the exact spectrum obtained numerically and blue dashed lines are the quasiclassical zeroth branches (25). Away from the level $\varepsilon = 0$, the correspondence of quasiclassical and exact spectra is of a very good accuracy. The splitting takes place in the small vicinity of $p_y = \pm p_y^*$ where the quasiclassical branch intersects the Fermi level. The behavior of spectral branches near this point is shown in the zoom inset in Fig. 6. All branches are discontinuous at $p_y = 0$ where they merge the continuum at $p_y = \pm 0$. Shown in Fig. 6 the spectrum of bound fermionic states at the domain wall in ^{3}He-A at $p_z = 0$ coincides with the spectrum of electronic states at domain walls in $p + ip$ superconductor Sr_2RuO_4.

IV. DISCUSSION

In contrast to the Fermi arcs on ^{3}He-A surface,[13] the Fermi arcs on the domain wall in ^{3}He-A and on the AB interface can not be obtained in the framework of quasiclassical approximation. Indeed, the quasiclassical approximation when applied to these systems yields that any of the subgap spectral branches given by Eq. (24) intersects the Fermi level.[25] Thus the number of zero modes in quasiclassics is model depended and does not satisfy the index theorem. The reason behind this discrepancy is that the zero modes exist for $p_x = 0$ [see dashed lines in Fig. 4(b)], which corresponds to the quasiclassical trajectories almost parallel to the plane of domain wall when one needs to get into account the normal reflection of quasiparticles from the order parameter inhomogeneity along the x axis. Since the normal reflection is inherently missing in quasiclassical Andreev equations (without diagonal potential), this approximation fails to describe zero modes and Fermi arcs on the domain wall in ^{3}He-A and the AB interface.

The modification of quasiclassical results due to the normal reflection can be analyzed by employing the semiclassical approximation (see Sec. III B 1), which yields three possible types of closed orbits in (p_x,x) phase space. In case when quasiclassical approximation is valid the regime (ii) of only Andreev reflection is realized with two separate orbits at $p_x > 0$ and $p_x < 0$ shown by the green solid lines in Fig. 4(a). The Bohr-Sommerfeld quantization (17) yields the same energy of bound states for the two orbits, which is degenerate by sign(p_x) and coincides well with quasiclassical result for $n_q > 0$. However, for smaller μ_x, two Andreev orbits merge into a single one shown in Fig. 4(a) by blue dash-dotted line. This orbit has both Andreev and normal reflection points and therefore is not described by the quasiclassical approximation. Moreover, merging of Andreev orbits doubles the orbit area. Therefore the number of subgap states according to Bohr-Sommerfeld quantization is doubled, which is manifested by the appearance of the second semiclassical branch in Fig. 4(b) simultaneously with merging of two Andreev orbits in Fig. 4(a). In exact spectrum obtained by solving numerically the BdG system the branch doubling is manifested in splitting of quasiclassical branches in Figs. 5 and 6. Thus the branch splitting is the direct result of normal reflection of quasiparticles moving almost parallel to the domain wall.

Affected by the enhanced normal reflection the behavior of the energy branches changes in $p_x \to 0$ limit qualitatively compared to the quasiclassical result. At a fixed value of momentum projection p_y (and spin projection σ_x in case of A phase domain wall), there is only one branch left, which intersects the Fermi level and supports Majorana states in accordance with the topological index theorem. The rest of spectral branches become non-monotonic at small values of $|p_x| = \sqrt{2m\mu_x}$ at $\mu_x > 0$ and turn upwards at $\mu_x < 0$ as can be seen in the Fig. 5.

V. CONCLUSION

We demonstrated that Fermi arcs on the domain wall in the A-phase and at the interface between the A and the B phases of superfluid ^{3}He obey the index theorem, which connects topological properties of bulk states on two sides of the walls with topology of zero-energy bound states. In contrast to the other systems supporting Fermi arcs, the bulk-edge correspondence here can be established only beyond the quasiclassical approximation by solving the exact BdG system numerically. The domain wall in A phase contains four Fermi arcs, if one takes into account spin degrees of freedom, while the AB interface contains two Fermi arcs, i.e., the same number as the surface of the A phase. The reason for this difference is that the Fermi arc is determined by the Weyl points in the bulk states on two sides of the wall. The ^{3}He-B, though being a topological superfluid, does not contain Weyl points and thus does not contribute to the number of the Fermi arcs. Note that the spectrum of localized fermions at the domain wall of the A phase is identical to the spectrum of electronic states bound at the domain wall in $p + ip$ superconductor Sr_2RuO_4.

Majorana fermions living on the Fermi arc at the AB interface may give an additional contribution to the calculated friction force acting on the moving interface[33] at very low temperatures. This is important for the development of the Kelvin-Helmholtz instability of the moving AB interface observed in Ref. 34 (see also Chap. 27 of Ref. 2). The latter instability has an analog with the ergoregion instability of black holes discussed in Chap. 32 of Ref. 2.

We considered the simplest most symmetric realizations of the A-A and A-B interfaces. The problem for future investigations is whether the Fermi arc survives or not, if the symmetry of the interface is violated. For that the relative homotopy group formalism applied to Green's function[35] is probably required.

ACKNOWLEDGMENTS

This work was supported, in part by the Academy of Finland (Centers of Excellence Programme 2012-2017), the EU 7th

Framework Programme (FP7/2007-2013, Grant No. 228464 Microkelvin), by Russian Foundation for Basic Research, Presidential RSS Council (Grant No. MK-4211.2011.2), by Programs of RAS "Quantum Physics of Condensed Matter" and "Strongly correlated electrons in semiconductors, metals, superconductors, and magnetic materials."

[1]C. D. Froggatt and H. B. Nielsen, *Origin of Symmetry* (World Scientific, Singapore, 1991).
[2]G. E. Volovik, *The Universe in a Helium Droplet* (Clarendon Press, Oxford, 2003).
[3]P. Hořava, Phys. Rev. Lett. **95**, 016405 (2005).
[4]D. B. Kaplan and Sichun Sun, Phys. Rev. Lett. **108**, 181807 (2012).
[5]M. A. Zubkov, Phys. Rev. D **86**, 034505 (2012).
[6]N. B. Kopnin and M. M. Salomaa, Phys. Rev. B **44**, 9667 (1991).
[7]G. E. Volovik, Pis'ma ZhETF **93**, 69 (2011) [JETP Lett. **93**, 66 (2011)].
[8]T. Meng and L. Balents, Phys. Rev. B **86**, 054504 (2012).
[9]T. T. Heikkilä, N. B. Kopnin, and G. E. Volovik, Pis'ma ZhETF **94**, 252 (2011) [JETP Lett. **94**, 233 (2011)].
[10]S. Ryu and Y. Hatsugai, Phys. Rev. Lett. **89**, 077002 (2002).
[11]A. P. Schnyder and S. Ryu, Phys. Rev. B **84**, 060504(R) (2011).
[12]G. E. Volovik, arXiv:1111.4627.
[13]Y. Tsutsumi, M. Ichioka, and K. Machida, Phys. Rev. B **83**, 094510 (2011).
[14]A. A. Burkov and L. Balents, Phys. Rev. Lett. **107**, 127205 (2011); A. A. Burkov, M. D. Hook, and L. Balents, Phys. Rev. B **84**, 235126 (2011).
[15]Xiangang Wan, A. M. Turner, A. Vishwanath, and S. Y. Savrasov, Phys. Rev. B **83**, 205101 (2011).
[16]P. Hosur, Phys. Rev. B **86**, 195102 (2012).
[17]T. L. Ho, J. R. Fulco, J. R. Schrieffer, and F. Wilczek, Phys. Rev. Lett. **52**, 1524 (1984).
[18]T. Ohmi, M. Nakahara, T. Tsuneto, and T. Fujita, Prog. Theor. Phys. **68**, 1433 (1982).
[19]M. M. Salomaa and G. E. Volovik, J. Low Temp. Phys. **74**, 319 (1989).
[20]G. E. Volovik, Pis'ma ZhETF **55**, 363 (1992) [JETP Lett. **55**, 368 (1992)].
[21]M. M. Salomaa and G. E. Volovik, Phys. Rev. B **37**, 9298 (1988).
[22]A. P. Schnyder, S. Ryu, A. Furusaki, and A. W. W. Ludwig, Phys. Rev. B **78**, 195125 (2008); AIP Conf. Proc. **1134**, 10 (2009).
[23]G. E. Volovik, Pis'ma ZhETF **90**, 639 (2009) [JETP Lett. **90**, 587 (2009)].
[24]M. Matsumoto and M. Sigrist, J. Phys. Soc. Jpn. **68**, 994 (1999).
[25]M. Nakahara, J. Phys. C **19**, L195 (1986).
[26]M. Ya. Azbel, ZhETF **59**, 295 (1970) [Sov. Phys. JETP **32**, 159 (1971)].
[27]H. So, Prog. Theor. Phys. **74**, 585 (1985).
[28]K. Ishikawa and T. Matsuyama, Z. Phys. C **33**, 41 (1986).
[29]K. Ishikawa and T. Matsuyama, Nucl. Phys. B **280**, 523 (1987).
[30]G. E. Volovik and V. M. Yakovenko, J. Phys.: Condens. Matter **1**, 5263 (1989).
[31]M. M. Salomaa, J. Phys. C **21**, 4425 (1988).
[32]N. Schopohl, Phys. Rev. Lett. **58**, 1664 (1987).
[33]N. B. Kopnin, ZhETF **92**, 2106 (1987) [Sov. Phys. JETP **65**, 1187 (1987)].
[34]R. Blaauwgeers, V. B. Eltsov, G. Eska, A. P. Finne, R. P. Haley, M. Krusius, J. J. Ruohio, L. Skrbek, and G. E. Volovik, Phys. Rev. Lett. **89**, 155301 (2002).
[35]J. I. Väyrynen and G. E. Volovik, Pis'ma ZhETF **93**, 378 (2011) [JETP Lett. **93**, 344 (2011)].